JACS
JOURNAL OF THE AMERICAN CHEMICAL SOCIETY

ARTICLE

pubs.acs.org/JACS

Exploring the First Steps in Core−Shell Electrocatalyst Preparation: In Situ Characterization of the Underpotential Deposition of Cu on Supported Au Nanoparticles

Stephen W. T. Price, Jonathon D. Speed, Prabalini Kannan, and Andrea E. Russell*

School of Chemistry, University of Southampton, Highfield, Southampton SO17 1BJ, United Kingdom

ABSTRACT: The underpotential deposition (upd) of a Cu shell on a non-Pt nanoparticle core followed by galvanic displacement of the Cu template shell to form core−shell electrocatalyst materials is one means by which the Pt-based mass activity targets required for commercialization of PEM fuel cells may be reached. In situ EXAFS measurements were conducted at both the Au L_3 and the Cu K absorption edges during deposition of Cu onto a carbon-supported Au electrocatalyst to study the initial stages of formation of such a core−shell electrocatalyst. The Au L_3 EXAFS data obtained in 0.5 mol dm^{-3} H_2SO_4 show that the shape of the Au core is potential dependent, from a flattened to a round spherical shape as the Cu upd potential is approached. Following the addition of 2 mmol dm^{-3} Cu, the structure was also measured as a function of the applied potential. At +0.2 V vs Hg/Hg_2SO_4, the Cu^{2+} species was found to be a hydrated octahedron. As the potential was made more negative, single-crystal studies predict an ordered bilayer of sulfate anions and partially discharged Cu ions, followed by a complete/uniform layer of Cu atoms. In contrast, the model obtained by fitting the Au L_3 and Cu K EXAFS data corresponds first to partially discharged Cu ions deposited at the defect sites in the outer shell of the Au nanoparticles at −0.42 V, followed by the growth of clusters of Cu atoms at −0.51 V. The absence of a uniform/complete Cu shell, even at the most negative potentials investigated, has implications for the structure, and the activity and/or stability, of the core−shell catalyst that would be subsequently formed following galvanic displacement of the Cu shell.

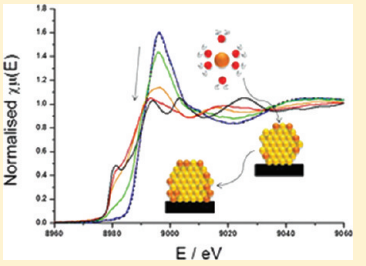

INTRODUCTION

The cost of platinum-containing electrocatalysts is one of the limiting factors that has slowed the uptake of low temperature fuel cells in important applications such as automotive power.[1−3] One means of reducing this cost is to effectively remove the unused Pt that lies below the surface layer of the metal nanoparticles by restricting the Pt to the surface in the shell of a core−shell catalyst. In recent years, the study and preparation of such core−shell nanoparticles for use as oxygen reduction reaction (ORR) catalysts have received considerable attention.[4−12] One method of preparing such core−shell catalysts that has been applied with success is the galvanic displacement of an underpotentially deposited (upd) Cu layer,[5−7,10−13] a reaction that proceeds spontaneously as the Cu^0 is oxidized by Pt^{2+} to leave Pt on the surface of core catalyst nanoparticles and allows complete removal of the Cu from the catalyst. By varying the size, shape, and composition of the core, the activity of the shell may be enhanced; for example, Adzic et al.[5] reported superior ORR activity for Pt shells on Au and Pd cores, with the best activity obtained when the lattice of the Pt shell is moderately compressed by interaction with the core.

Studies at single-crystal electrode surfaces, where the surface termination is well-defined,[14−16] have provided a basis for the understanding of adsorption sites on electrode surfaces and, if stepped surfaces are studied, the role of undercoordinated surface atoms at the step edges in determining activity and the initial stages of monolayer formation.[17−20] Cu upd on Au surfaces from a sulfate supporting electrolyte is one of the more extensively studied upd systems, and the process of deposition on Au(111) surfaces is well-documented.[13,17−27] During the initial stages of Cu deposition on Au(111), it has been shown that the sulfate anion is coadsorbed with the Cu onto the Au surface[25,28] (depicted schematically in Figure 1a) and that the Cu still retains a partial, yet unknown, charge. Surface X-ray scattering (SXS) combined with scanning tunneling microscopy (STM) and atomic force microscopy (AFM) have shown that during the initial deposition stage of Cu on Au(111) surfaces in acidic medium, the Cu atoms and sulfate ions both occupy 3-fold hollow sites.[29,30] EXAFS studies by Lee et al.[22] of Cu upd on Au(111) gave results consistent with the model of Cu coadsorbed with sulfate, in which one-third of the 3-fold adsorption sites in the ordered layer were occupied by sulfate ions. Thus, in Figure 1a, the coadsorbed sulfate ions are sitting within the Cu upd layer with coverage $\theta_{Cu} = 0.66$. At more negative potentials (before the bulk deposition), they found that the surface structure rearranged to be a complete Cu monolayer of Cu with the sulfate anions now occupying 3-fold sites on top of the Cu adlayer (Figure 1b) with coverage $\theta_{Cu} = 1$. The adsorption of Cu in 2-fold and atop sites was also investigated in their study; however ,the quality of the EXAFS fit was noticeably reduced in both cases, indicating that these adsorption sites were less favored than the 3-fold site.

Cu upd on the Au(110) and (100) surfaces has also been reported.[20,31−34] The Cu upd adlayer occupies 4-fold sites on both surfaces, forming a pseudomorphic overlayer. In contrast to

Received: July 20, 2011
Published: October 27, 2011

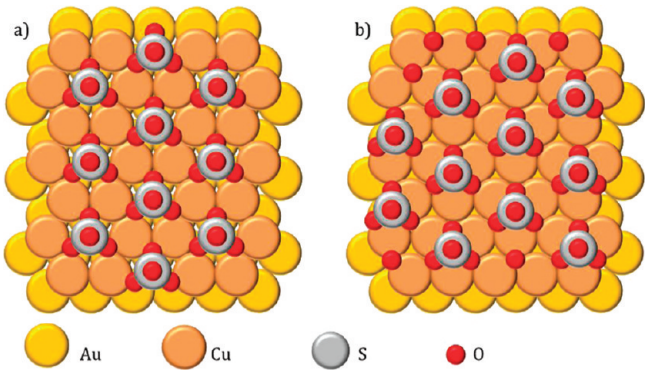

Figure 1. Schematic of deposition of Cu on Au(111) with sulfate anions: (a) first stage and (b) full Cu monolayer.

the Au(111) surface, $\theta_{Cu} = 1$ over the entire upd range. As for the Au(111) surface, a sulfate adlayer atop the Cu adlayer is also likely to be present.[32,33] Kuzume et al.[20] also investigated Cu upd on higher index Au including (332), (755), (775), and (554) surfaces. The increasing terrace width on these surfaces was found to correlate with sharper peaks, indicating more clearly defined deposition. These higher index planes have terraces with a (111) structure, and steps that resemble the (110) structure, the resulting voltammetry bearing similarities to both.

In seeking a means of preparing core−shell electrocatalysts, the first reports of the use of displacement of a Cu upd monolayer by Pt^{2+} cations by Brankovic, Wang, and Adzic described the modification of a Au(111) surface and the effects of the underlying Au surface on the hydrogen adsorption behavior of the Pt.[13,35] These studies showed two clearly resolved Cu upd peaks, in agreement with the previously reported work[29] described above. Subsequent STM measurements showed that the Pt layer formed upon displacement of the upd Cu consisted of a 2D monolayer of partially interconnected nanoclusters of monatomic height and reported enhanced oxygen reduction activity, attributed to a decrease in adsorption of OH.[36] Importantly, none of these studies of Pt deposition on to Au(111) surfaces showed a smooth, epitaxial Pt deposit following the displacement of the Cu upd layer in a single cycle.

Practical electrocatalysts for use in fuel cells consist of high surface area materials, usually carbon-supported metal nanoparticles, and the initial studies of Pt monolayer catalysts were extended to carbon-supported nanoparticles using a variety of core catalysts.[5,6,10,37] The focus of these reports was on the demonstration of the enhanced Pt mass activity, current per gram of Pt, of the resulting core−shell catalysts for, primarily, the oxygen reduction reaction to illustrate the reduced costs of the materials over a pure Pt/C catalyst. Structural characterization of the core−shell catalysts has not been widely reported, and that which has, has largely relied on TEM images of varying resolution, with recent results showing a clearly defined core−shell structure for Pt deposited on PdIr/C[10] using high-resolution TEM and for Pt on Pd/C from HAADF-STEM images.[5,38] Interestingly, Wang et al.[5] acknowledge that it was only possible to obtain such well-defined core−shell structures by modifying the Cu upd displacement procedure. To ensure complete encapsulation of the Pd core, which is not stable in the acid electrolyte at potentials where oxide formation takes place, the Cu upd layer was repeatedly formed and removed in a solution containing 50 mM H_2SO_4 and 50 mM $CuSO_4$ in the presence of 0.1 mM K_2PtCl_6. This deposition and removal of the Cu upd layer was thought to lower the Pt deposition rate so that a smooth Pt layer formed. The completeness of the Pt shell has been identified as an important feature in the stability of such core−shell catalysts;[5,39] thus obtaining such a smooth shell is important to the eventual use of the materials in a working fuel cell.

As exemplified by the article by Solla-Gullón et al.,[15] the information obtained from single-crystal studies is now being used to provide a detailed interpretation of the electrochemical behavior of nanoparticles as, particularly for Pt, these can be described as consisting of small (111) and (100) domains.[40] The structural information obtained from the Au single-crystal studies of Cu upd and the initial studies of Pt^{2+} displacement, described above, has informed the subsequent development of the core−shell nanoparticle catalysts. However, it is not clear that Cu upd on nanoparticles is adequately modeled by such single-crystal studies.

In contrast to the detailed studies of Cu upd on Au single-crystal surfaces, the structural characterization of Cu upd on Au nanoparticles has received far less attention. XPS has been used ex situ to study a Au/C catalyst modified by the Cu upd layer, and then following displacement of the layer by Pt to produce the core−shell material.[41] The XPS signal from the Cu layer was only just above the noise level, reflecting its ultrathin nature, and did not provide the level of structural detail needed to determine the adsorption sites of the Cu or its coverage. A recent theoretical study reported by Oviedo et al.[8] identified the number of upd adsorption sites on ideal truncated octahedral Au nanoparticles and how these varied as a function of the nanoparticle radius. On the basis of this model, the total Cu upd coverage on an idealized Au nanoparticle would be expected to be less than the total number of Au surface atoms available, corresponding to less than a full outer shell of Cu atoms, although a uniform surface coverage could still be achieved. The functions proposed by Oviedo predict a maximum coverage of 0.75 of a monolayer for a 1289 atom (truncated cuboctahedron) Au nanoparticle, with an approximate diameter of 4.3 nm, and that full monolayer coverage would only be obtained when the deposition is driven beyond the onset of bulk deposition. For smaller nanoparticles, the theoretical upd coverage is even less.

Cu upd on Au nanorods was investigated by Seo et al.[42] as a means to determine surface morphology, noting the overlap in the Cu deposition peaks between Au(111) and (100). The nanorods used have dimensions of 100−200 nm with well-defined crystal surfaces and, therefore, have more in common with single-crystal surfaces than the much smaller nanoparticles used in this study. Ag and Pb upd have been more extensively studied[43−48] than Cu upd on shape-controlled Au nanocubes, nanorods, and nanocrystals with both (111) and (100) surfaces; however, these again have dimensions on the order of 50−200 nm bearing more in common with single crystals than nanoparticles. With decreasing particle sizes, the definition of the upd peaks was more poorly defined due to the lower size of surface domains, hindering any quantitative determination of the surface.[20,44]

In this study, we present the first in situ structural study of Cu upd on carbon-supported Au nanoparticle catalysts using extended X-ray absorption fine structure (EXAFS), examining the initial stages of formation of the Cu upd adlayer. EXAFS has proven to be a powerful and flexible characterization technique and has been applied to studies of heteroepitaxial film growth,[21−23] nanoparticle characterization,[49−51] and potential-dependent studies of electrocatalysts.[52−54] The in situ EXAFS measurements presented here are unique in their ability to provide a structural model at each stage of the deposition of Cu on Au nanoparticles during the

deposition. By collecting the data at both the Au L_3 and the Cu K absorption edges, the structural model is constructed from the perspective of both the Cu and the Au atoms, providing a more complete picture. In agreement with the calculations of Oveido et al. described above, and in contrast to the previous single-crystal studies that form the basis of the current models of such core−shell electrocatalysts, the EXAFS analysis confirms that a complete/uniform Cu shell was not achieved. The structural information presented here for Cu upd on nanoparticle Au catalysts will, therefore, enable the development of better models and further understanding of the preparation, activity, and stability of such core−shell catalysts.

METHODS

Catalyst Preparation. The Au nanoparticles were prepared by the thiol encapsulation method of Brust et al.,[55] which has become one of the standard preparation methods. To prepare the carbon-supported electrocatalyst, the Au colloid dispersion and a suspension of Vulcan carbon XC-72 R were combined in ethanol. The mixture was sonicated for 30 min and refluxed at 80 °C under vigorous stirring for 10 h. The resulting powder was separated by filtration and then thoroughly washed with purified water, before being dried at 110 °C for 2 h.

Electrode Preparation. The required amount of catalyst (approximately 60 mg) was finely ground and then dispersed in a small amount of deionized water (0.75 mL) and isopropanol (0.20 mL). Nafion (10.85 wt % solids in water) was added to the solution to give an ink with 30 wt % Nafion solids when dry. The mixture was sonicated for 20 min followed by mixing with a Fisher PowerGen 125 homogenizer. The resulting mixture was painted onto carbon paper (TGP-H-060), which was dried, weighed, and the process repeated until the desired loading of 0.07 mg cm^{-2} Au was obtained. The electrodes were then pressed at 177 °C and 1 bar for 3 min. 1.32 cm^2 circular button electrodes were cut from the sheet and hydrated by boiling in deionized water prior to use.

Electrochemistry. An in situ electrochemical cell was used to collect XANES and EXAFS data during the upd of Cu on Au. The working electrode (WE) was held in place by a Au wire contact, a Pt wire served as the counter electrode (CE), and the reference electrode (RE) was a mercury mercurous sulfate (MMS), Hg/Hg_2SO_4, electrode that was connected to the cell via a short length of tubing containing the electrolyte. The cell was controlled by a μAutolab type III potentiostat running the General Purpose Electrochemistry Software 4.9 (GPES). The 0.5 M H_2SO_4 electrolyte was purged with N_2 and then pumped through the cell using a peristaltic pump.

The prepared electrodes were cycled in 0.5 M H_2SO_4 from −0.65 to 0.9 V vs MMS, until subsequent voltammograms overlaid, to clean the surfaces of any residual thiols from the synthesis. Previously reported studies of Cu upd on Au[13,22,23,29] have used Cu^{2+} solutions containing between 0.02 mM and 0.1 M Cu^{2+}, in 0.1−1 M H_2SO_4 concentrations. For this study, 2 mM $CuSO_4$ was chosen to ensure there was enough Cu^{2+} in the volume of the solution in the cell to give a full theoretical monolayer coverage Cu on the Au nanoparticles, while being dilute enough so that there was minimal Cu^{2+} left in solution after the deposition, as the latter would complicate the EXAFS analysis (due to the small amount of sample in the X-ray beam).

Voltammograms were collected before and after the potential holds for the EXAFS measurements at +0.20, −0.21, −0.42, and −0.51 V vs MMS in 0.5 M H_2SO_4. The procedure for collection of the EXAFS during upd Cu deposition in 2 mM $CuSO_4$ in 0.5 M H_2SO_4 (purged with N_2) was modified to include an 20 min potential hold prior to EXAFS data collection to ensure complete adlayer formation. The Cu^{2+} concentration was sufficient to ensure a complete monolayer coverage based on the in situ cell volume alone (∼1 mL), and the excess in the electrolyte being pumped through the cell was nearly 2000 times that for a monolayer coverage, sufficient for bulk deposition of Cu on the nanoparticles.

Electron Microscopy Measurements. Powder samples of the Au/C catalyst for TEM-EDX using a Tecnai F20 transmission electron microscope were crushed between two glass slides, and samples were positioned onto a lacey carbon coated Cu "finder" grid with the aid of a micromanipulator. The microscope was operating with a voltage of 200 kV and C2 apertures of 30 and 50 m.

X-ray Diffraction Measurements. The XRD analysis used a Bruker AXS D8 Advance diffractometer in parallel beam mode with a 60 mm Gobel mirror, and a Ni filtered Cu K_α X-ray source. XRD patterns were collected over a scan range of 10−140° 2Θ with a 0.022° step size at a scan rate of 0.264° 2Θ per minute, and the diffracted beam was collected using a Vantec Position Sensitive Detector.

X-ray Absorption Measurements. X-ray absorption measurements were recorded at the Cu K absorption edge (8979 eV) and the Au L_3 absorption edge (11919 eV) at beamline X23A2 of the National Synchrotron Light Source (Brookhaven National Laboratory, U.S.) with ring energy 2.58 GeV and a current of 220−290 mA. The station operated with an upward reflecting, fixed exit Golovchenko−Cowan design monochromator containing Si(311) crystals stabilized by piezo-electric feedback with a single bounce harmonic rejection mirror to reduce higher harmonics. The catalyst powder sample was measured in transmission mode using 20% Ar/80% N_2 filled ion chambers after cooling to 85 K using a displex unit, and the in situ electrode measurements in fluorescence mode at 300 K using a 4-element silicon drift detector. Calibration of the monochromator was carried out using Cu foil and Au foil.

Data Analysis. The acquired data were processed and analyzed using the programs Athena and Artemis,[56] which implement the FEFF6 and IFEFFIT codes.[57,58] The AUTOBK method[59] was used to isolate the *k*-space EXAFS data from the raw data, and a theoretical EXAFS signal was constructed using FEFF6. Data were collected for a Au foil prior to the nanoparticle measurements to enable determination of the amplitude reduction factor. This was found to be 0.85 ± 0.04; all coordination numbers and subsequent results were corrected accordingly. To fit the Au L_3 absorption edge data, the theoretical signal included single and multiple scattering contributions up to the third nearest neighbor in the Au face centered cubic (fcc) structure with a *k* range of 3−16 $Å^{-1}$ (with the exception of the 85 K measurement, which was fit up to 18 $Å^{-1}$) and an *R* range of 1.8−5.5 Å. The single scattering paths to the nearest three neighbors were $[Au_{abs}-Au_1-Au_{abs}]$, $[Au_{abs}-Au_2-Au_{abs}]$, and $[Au_{abs}-Au_3-Au_{abs}]$, where abs denotes the absorbing atom and the numeric subscripts identify Au the first three Au neighbor distances in the fcc structure (i.e., Au_1 is first nearest neighbor, Au_2 is second nearest neighbor, etc.). Also included were noncollinear multiple scattering paths $[Au_{abs}-Au_1-Au_1-Au_{abs}]$ and $[Au_{abs}-Au_3-Au_1-Au_{abs}]$. The path degeneracy was left to vary as a fitting parameter to account for the undercoordination of the surface atoms. Mean square disorder parameters were constrained on the basis of the photoelectron mean free path length. The nearest neighbor distances were constrained to an isotropic expansion factor, and a single photoelectron energy correction was applied to all paths. The selection of paths chosen is similar to those used in the study of other nanoparticle systems.[60,61]

The Cu K absorption edge data were fit between 3 and 11 $Å^{-1}$ in *k* space and 1−3 Å in *R* space, including the first nearest neighbors only. A Cu foil reference was measured, as was a 2 mM $CuSO_4$ reference sample. An S_0^2 of 0.82 ± 0.20 was determined from a 2 mM $CuSO_4$ solution reference sample and 0.89 ± 0.05 from the Cu foil. Fitting models were based on a fcc Cu foil and a fcc 1:1 Cu:Au alloy for the potentials corresponding to Cu upd, and an octahedral Jahn−Teller distorted $Cu(H_2O)_6$ solvated copper ion[62−64] for the Cu^{2+} in the electrolyte. As with the Au fitting model, the path degeneracy was allowed to vary with

the fit along with a bond length correction, mean square disorder, and photoelectron energy correction.

RESULTS AND DISCUSSION

Au/C Core Catalyst Characterization. Prior to investigation of the Cu upd, the Au/C catalysts were characterized using TEM, XRD, and EXAFS at the Au L_3 edge, to confirm the dispersion of the Au nanoparticles on the carbon support and to provide a basis for comparison of the structure obtained after Cu upd.

Figure 2 shows a bright field micrograph of the as-prepared Au nanoparticles with the associated particle size distribution. TEM shows the Au nanoparticles to be well dispersed on the carbon support, with relatively evenly shaped particles. The size distribution is narrow, with a volume weighted average particle diameter of 2.40 nm. EDX confirmed that the particles consisted of Au, but S was not detected in the areas imaged.

The XRD pattern (Figure 3) is dominated by the carbon support, due to both the low Au loading and the poorly crystalline nature of the Au nanoparticles. The volume weighted Rietveld determined average crystallite size was 2.41 nm, in good agreement with the TEM determined particle size.

Figure 4 displays the ex situ k^3 weighted EXAFS data and corresponding Fourier transform at 85 K of the as-prepared catalyst powder obtained at the Au L_3 edge. The fit parameters corresponding to the plots in Figure 4 are presented in Table 1.

A roughly spherical shape can be inferred from the ratio of the third to first shell coordination numbers measured by EXAFS, and these numbers may be used to provide an estimated particle diameter of 1.5 nm, using the models proposed by Jentys.[66] The degree of disorder present reported here as the σ^2 term in the fit is somewhat large considering the measurement temperature. Work by Solliard[67] has shown that, while Pt nanoparticles retain their monocrystalline structure down to approximately 1 nm, Au nanoparticles below 6 nm are better represented as aggregates of polytetrahedral grains. The increased disorder observed in the EXAFS is, therefore, attributed to this structural reorganization, which is also observed as poor crystallinity in the XRD pattern.

EXAFS is a per atom averaging technique, and, therefore, the contributions from any partially formed nanoparticles, clusters or single Au atoms on the support, are counted toward the average coordination number. These fragments would be missed by XRD due to the lack of any long-range order and would not be visible to routine TEM imaging, resulting in the average particle size determined by EXAFS, 1.5 nm, being lower than the 2.4 nm diameter found using TEM and XRD.

While EDX detected no S in the area examined, the presence of a Au−S first shell scattering path was needed to improve the quality of the EXAFS fit. This was attributed to some of the thiol encapsulating layer remaining after immobilization of the particles on the Au support.

These results confirm that the as-prepared catalyst consisted of well-dispersed Au particles, with an average diameter between 2 and 3 nm, in agreement with the preparation method used. Additionally, the EXAFS data indicate that some of the thiol used to restrict the growth of the particles during their preparation was retained on the surface.

Electrochemistry. The potentials at which Cu upd occurred were determined using cyclic voltammetry, as has previously been reported in the studies of Cu upd on Au surfaces.[13,20,29,32,33,35] Figure 5 shows the cyclic voltammograms in 0.5 M H_2SO_4

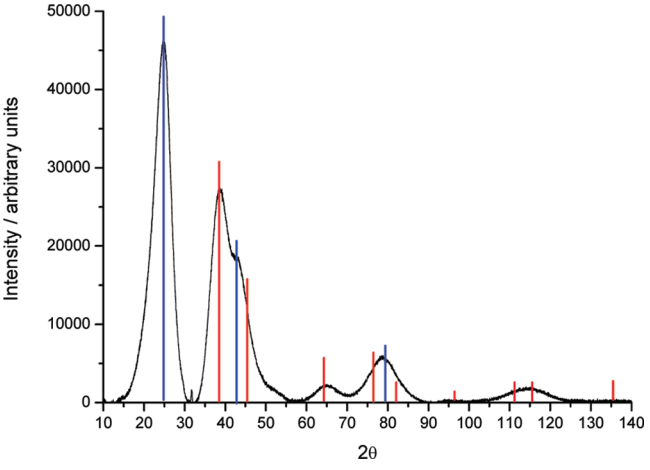

Figure 3. XRD patterns of the 4 wt % Au/C catalyst powder. Data are the black line, red vertical bars are the reference positions of reflections from cubic Au (PDF no. 03-065-2870, a = 4.08 Å), and the blue vertical bars are those for the carbon support.

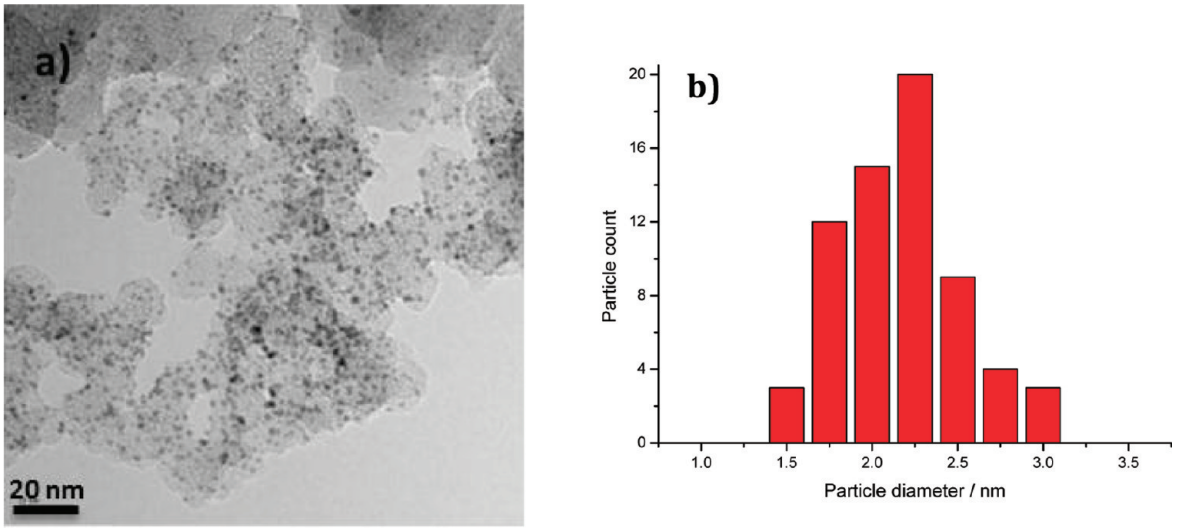

Figure 2. (a) TEM micrographs of the 4 wt % Au/C catalyst powder and (b) the particle size distribution determined by analysis of the TEM image.

dx.doi.org/10.1021/ja206763e |J. Am. Chem. Soc. 2011, 133, 19448–19458

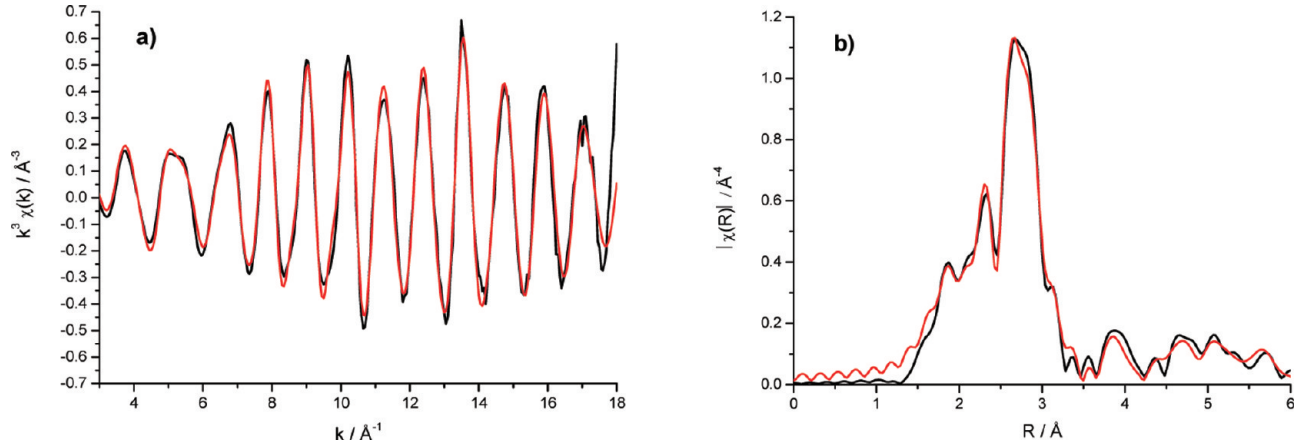

Figure 4. (a) k^3 weighted experimental data (black) and fit (red) and (b) the corresponding k^3 weighted Fourier transform for the 4 wt % Au/C catalyst powder as a self-supporting BN pellet at 85 K.

(black line) and following the addition of 2 mM $CuSO_4$ (red line) obtained for (a) a polycrystalline Au disk electrode and (b) the Au/C catalyst electrode. In the voltammograms for the Au disk, the peak at −0.21 V represents the first deposition stage, previously attributed to an adlayer structure involving both the Cu atoms and the SO_4^{2-} anions,[29] followed by a complete Cu adlayer deposition at −0.42 V. Bulk deposition of Cu occurs by −0.51 V. The deposition and stripping peaks for the Au/C catalyst electrode in the in situ cell are not as well-defined as for the Au disk, with only two broad peaks being observed in each direction rather than three. Previous reports of upd on Au nanorods[42] and nanocrystals[44] have used the position and shape of the upd peaks to identify the crystalline plane of the surface facets. Because of the broad nature of the upd peaks observed in our study (Figure 5b), which is attributed to the small size of the nanoparticles as compared to those reported in previous studies, identification of the particular surface facet was not possible. In comparison to the Au disk, the voltammogram is dominated by capacitance, which is associated with the carbon support and the electrode structure, as the Au loading of the catalyst was restricted to 4 wt % to ensure a narrow particle size distribution. The redox couple observed in the acid CV between −0.3 and 0.1 V has previously been attributed to quinone groups on the surface of the carbon support.[68]

In Situ Au L_3 Edge EXAFS in 0.5 M H_2SO_4. Prior to investigating the effects of Cu upd on the structure of the catalyst nanoparticles, the effects of the applied potential on the structure of the Au/C core catalyst were explored. Figure 6 displays k^3 weighted Au L_3 EXAFS data acquired at 300 K in the in situ electrochemical cell and the corresponding Fourier transforms. The fit parameters corresponding to the plots in Figure 6 are presented in Table 2.

The average first shell coordination number obtained in situ, 10.1, is significantly larger than that for the as-prepared sample obtained ex situ and corresponds to an average particle diameter of 3.8 nm. This increase is attributed to the effects of electrochemical pretreatment prior to collecting the EXAFS data; the prepared electrode was cycled in 0.5 M H_2SO_4 until there was no change in the shape of the oxide formation or stripping peaks (i.e., the scans overlaid). This cycling process appears to cause aggregation of nanoparticles and fragments in close proximity, resulting in the increase in coordination numbers, and therefore particle size, observed.

Table 1. Structural Parameters Obtained by Fitting the Au L_3 Edge EXAFS Data Shown in Figure 4[a]

shell	N	R/Å	$\sigma^2 \times 10^4$/Å^2	ΔE_0/eV	R_f
Au−Au_1	6.9 ± 0.4	2.85 ± 0.01	56 ± 2	6.4 ± 0.3	0.017
Au−S_1	1.0 ± 0.3	2.31 ± 0.01	83 ± 37		
Au−Au_2	1.5 ± 0.7	4.03 ± 0.01	59 ± 25		
Au−Au_3	11.0 ± 3.8	4.94 ± 0.01	104 ± 23		

[a] N is the coordination number, R is the coordination distance, σ^2 is the Debye Waller (disorder) term, ΔE_0 is the shift in the Fermi energy, and R_f is a measure of the goodness of fit.[65]

The second coordination shell in the EXAFS data proved difficult to fit in all cases, with both amplitude and disorder terms being small, and the respective errors large. Both Au−S and Au−O scattering paths could not be fit to the data and, therefore, were not the cause of the poor fit. These scattering paths were considered because of the thiol used during the nanoparticle synthesis and the H_2SO_4 electrolyte. The lack of an Au−S scattering contribution indicates that the cycling removed the thiol from the surface of the nanoparticles.

The ratio between the first and third shell coordination numbers at +0.20 V is near 1, due to the low third shell coordination. This low ratio is attributed to a flattening of the particles on the surface of the support.[66] At all of the negative potentials, the third shell coordination number is larger, with the ratio of first to third shell coordination numbers being greater than 2, and this is attributed to a return to an approximately spherical particle shape as observed for the as-prepared sample. Thus, the shape of the Au nanoparticles is potential dependent, with reorganization of the Au nanoparticles occurring between +0.20 and −0.21 V. This potential-dependent fluctuation in the shape of the Au nanoparticles limits the applicability of models that describe the surface of such particles as fixed facets with defined (111) or (100) termination.

In Situ Au L_3 Edge EXAFS in 0.5 M H_2SO_4 and 2 mM $CuSO_4$. The effects of Cu upd on the structure were first determined from the perspective of the Au core atoms by examining data collected at the Au L_3 edge. Figure 7 displays the k^3 weighted Au L_3 EXAFS data acquired at 300 K in the in situ electrochemical cell and the corresponding Fourier transforms. The fit parameters corresponding to the plots in Figure 7 are presented in

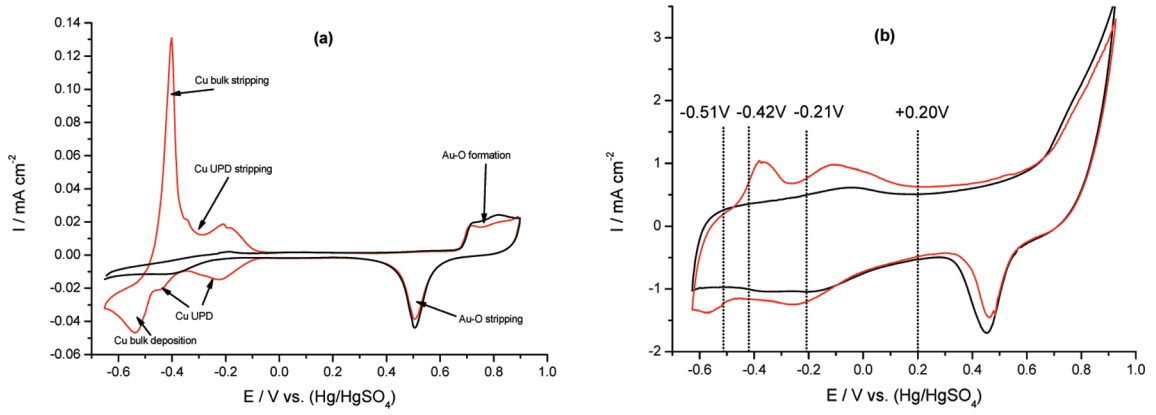

Figure 5. Cyclic voltammograms of (a) 0.196 cm^2 Au disk electrode and (b) 4 wt % Au/C catalyst electrode (1.32 cm^2) in 0.5 M H_2SO_4 (black) and following the addition of 2 mM $CuSO_4$ (red) at 10 mV s^{-1}. The dashed vertical lines in (b) indicate the potentials at which the in situ EXAFS data were collected.

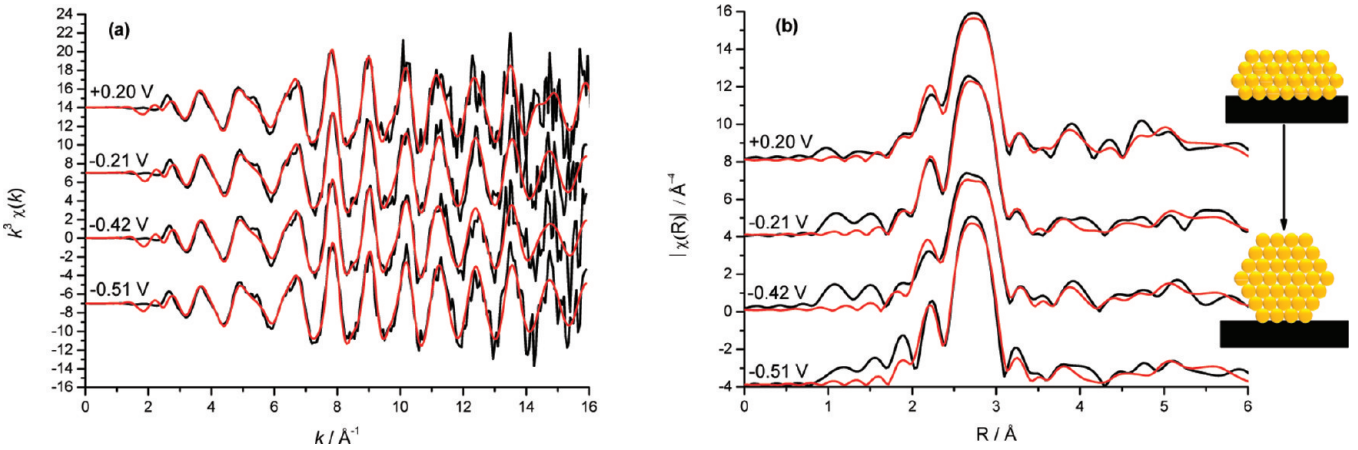

Figure 6. (a) k^3 weighted Au L_3 edge experimental data (black) and fit (red) and (b) the corresponding k^3 weighted Fourier transforms for the 4 wt % Au/C electrode in 0.5 M H_2SO_4 as a function of the applied potential, with a schematic of the Au (yellow) on carbon (black) particle shape shown in the right-hand margin.

Table 2. Structural Parameters Obtained by Fitting the Au L_3 Edge Data Shown in Figure 6

V vs (Hg/HgSO$_4$)	shell	N	R/Å	$\sigma^2 \times 10^4$/Å^2	ΔE_0/eV	R_f
+0.20	Au−Au$_1$	10.3 ± 0.8	2.85 ± 0.01	85 ± 5	3.7 ± 0.5	0.033
	Au−Au$_2$	0.7 ± 0.8	4.04 ± 0.01	15 ± 36		
	Au−Au$_3$	11.3 ± 6.5	4.95 ± 0.01	94 ± 34		
−0.21	Au−Au$_1$	10.1 ± 0.6	2.85 ± 0.01	81 ± 4	5.0 ± 0.4	0.023
	Au−Au$_2$	1.4 ± 1.4	4.03 ± 0.01	82 ± 71		
	Au−Au$_3$	21.3 ± 13.1	4.93 ± 0.01	150 ± 48		
−0.42	Au−Au$_1$	10.2 ± 0.7	2.85 ± 0.01	86 ± 5	4.6 ± 0.4	0.026
	Au−Au$_2$	0.6 ± 1.0	4.03 ± 0.01	32 ± 63		
	Au−Au$_3$	21.2 ± 12.4	4.93 ± 0.01	137 ± 42		
−0.51	Au−Au$_1$	9.7 ± 0.7	2.85 ± 0.01	78 ± 4	4.3 ± 0.4	0.027
	Au−Au$_2$	1.2 ± 1.4	4.02 v 0.01	61 ± 55		
	Au−Au$_3$	21.5 ± 13.8	4.93 ± 0.01	148 ± 49		

Table 3. A reduced k range of 3−14 Å^{-1} was used in fitting the data obtained at +0.20 V, due to poorer data quality above k = 14 Å^{-1}.

As was the case with the Au L_3 edge measurements in H_2SO_4 alone, the particles are flattened out on the support at positive potentials, and more spherical at negative potentials, and once again the second shell coordination number proved difficult to fit.

Attempts were made to fit Au−O and Au−S scattering paths to all data sets, but their inclusion made no physically realistic

dx.doi.org/10.1021/ja206763e |J. Am. Chem. Soc. 2011, 133, 19448–19458

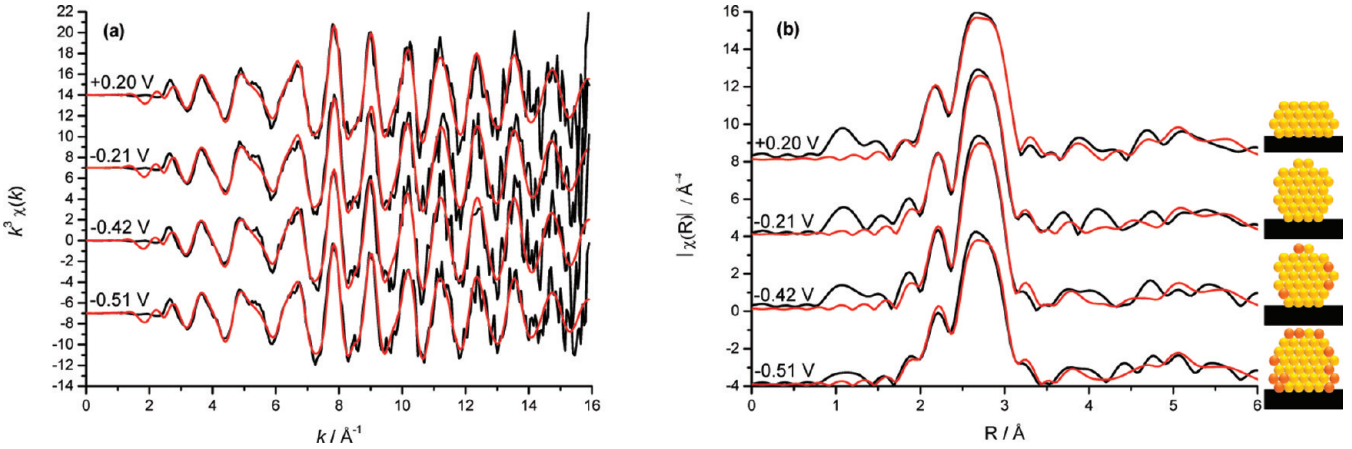

Figure 7. (a) k^3 weighted Au L_3 edge experimental data (black) and fit (red) and (b) the corresponding k^3 weighted Fourier transform for the 4 wt % Au/C electrode in 0.5 M H_2SO_4 and 2 mM $CuSO_4$ as a function of the applied potential, with a schematic of the Cu (orange) deposition on the carbon-supported Au (yellow) particles shown in the right-hand margin.

Table 3. Structural Parameters Obtained by Fitting the Au L_3 Edge Data Shown in Figure 7

V vs ($Hg/HgSO_4$)	shell	N	R/Å	$\sigma^2 \times 10^4$/Å^2	ΔE_0/eV	R_f
+0.20	Au−Au_1	10.5 ± 0.7	2.85 ± 0.01	82 ± 4	4.5 ± 0.4	0.018
	Au−Au_2	1.7 ± 1.7	4.03 ± 0.01	99 ± 83		
	Au−Au_3	13.8 ± 7.2	4.94 ± 0.01	107 ± 32		
−0.21	Au−Au_1	10.3 ± 0.8	2.85 ± 0.01	81 ± 5	4.3 ± 0.5	0.029
	Au−Au_2	3.7 ± 4.0	4.03 ± 0.01	183 ± 179		
	Au−Au_3	22.2 ± 14.9	4.94 ± 0.01	158 ± 53		
−0.42	Au−Au_1	10.4 ± 0.8	2.85 ± 0.01	79 ± 4	3.7 ± 0.5	0.028
	Au−Au_2	2.1 ± 2.1	4.03 ± 0.01	90 ± 65		
	Au−Au_3	18.6 ± 13.1	4.94 ± 0.01	136 ± 51		
−0.51	Au−Au_1	11.0 ± 0.7	2.85 ± 0.01	87 ± 4	4.4 ± 0.4	0.023
	Au−Au_2	2.0 ± 2.0	4.03 ± 0.01	97 ± 71		
	Au−Au_3	20.6 ± 9.9	4.94 ± 0.01	126 ± 33		

improvements to the fit, indicating that none of the thiol remained and that a sulfate ion containing adlayer was not formed. Much more interestingly, however, the addition of a Au−Cu first shell scattering path at negative potentials, where the voltammograms indicated the formation of the Cu upd layer, also failed to produce a physically realistic fit. In an attempt to investigate this further, the upper k limit over which the data were fitted was reduced to minimize the relative contribution of the Au and increase the relative Cu contribution to the back-scattering amplitude, as the backscattering of the lighter element peaks at lower k values, while that of Au is greater at larger k values. This also resulted in no change to either the overall fit quality or the physical viability of the scattering path. The absence of a Cu contribution will be discussed in more depth after the Cu K edge data are presented below, but to summarize at this point, the data indicate that even at the most negative potential explored in this study, −0.51 V, a complete Cu layer is not formed on the Au core, in contrast to the epitaxial/pseudomorphic Cu upd layer reported in studies of the single-crystal surfaces discussed in the Introduction.

In Situ Cu K Edge XANES and EXAFS in 0.5 M H_2SO_4 and 2 mM $CuSO_4$. The structure of the Cu upd layer was further investigated by collecting the XAS data from the perspective of the Cu atoms at the Cu K edge. Both the XANES region, used to determine the oxidation state of the Cu species as a function of the applied potential, and the EXAFS region of the data were analyzed.

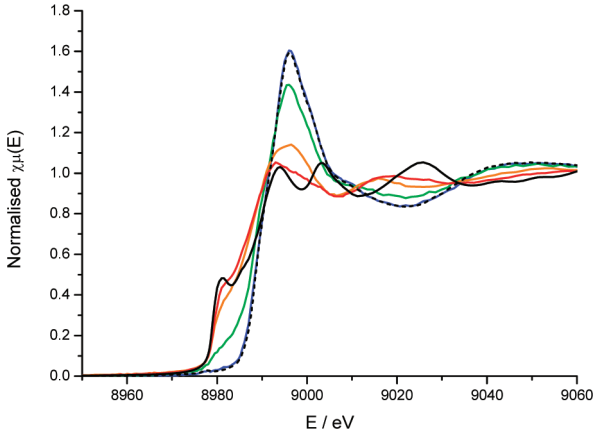

Figure 8. Cu K edge XANES. Cu foil (−), 2 mM $CuSO_4$ reference solution (- - -), and 4 wt % Au/C electrode in 0.5 M H_2SO_4 and 2 mM $CuSO_4$ at +0.20 V (blue), −0.21 V (green), −0.42 V (orange), and −0.51 V (red).

dx.doi.org/10.1021/ja206763e |J. Am. Chem. Soc. 2011, 133, 19448–19458

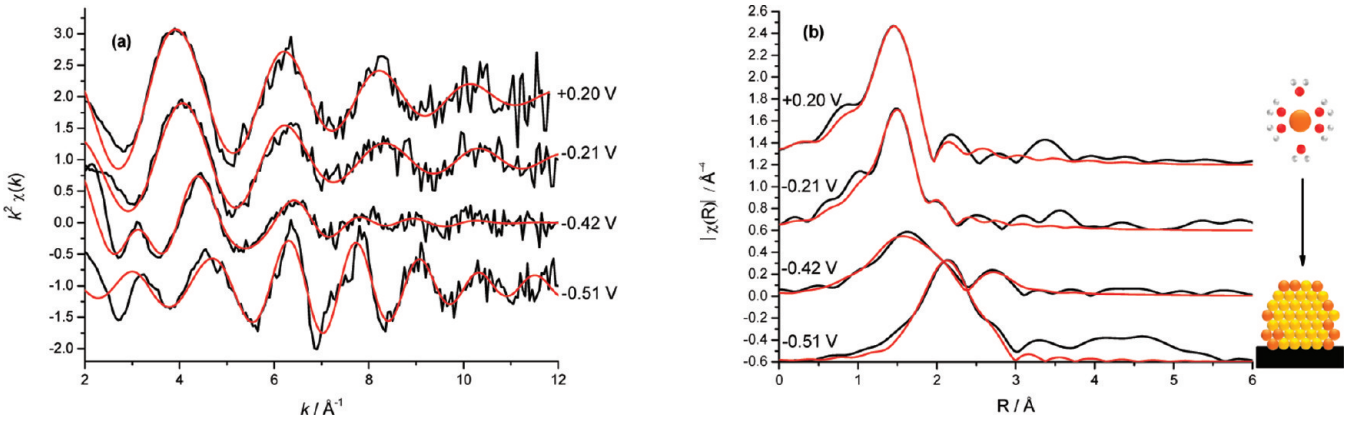

Figure 9. (a) k^2 weighted Cu K edge experimental data (black) and fit (red) and (b) the corresponding k^2 weighted Fourier transforms for the 4 wt % Au/C electrode in 0.5 M H_2SO_4 and 2 mM $CuSO_4$ as a function of the applied potential, with a schematic of the solvated Cu ion and final Cu modified Au/C particle shown in the right-hand margin.

Table 4. Structural Parameters Obtained by Fitting the Cu K Edge Data Shown in Figure 9

V vs ($Hg/HgSO_4$)	shell	N	R/Å	$\sigma^2 \times 10^4$/Å^2	ΔE_0/eV	R_f
+0.20	Cu−O_{eq}	4.5 ± 1.8	1.96 ± 0.02	70 ± 31	−7.5 ± 2.6	0.010
	Cu−O_{ax}	2.3 ± 0.9	2.33 ± 0.04	63 ± 65		
−0.21	Cu−O_{eq}	3.2 ± 0.3	1.94 ± 0.01	46 ± 14	−5.8 ± 1.4	0.010
	Cu−O_{ax}	2.0 ± 0.2	2.50 ± 0.04	58 ± 63		
−0.42	Cu−O	2.3 ± 0.9	1.93 ± 0.02	219 ± 47	−1.0 ± 2.2	0.037
	Cu−Cu					
	Cu−Au	6.4 ± 2.4	2.60 ± 0.03	219 ± 53		
−0.51	Cu−O				−4.3 ± 3.1	0.024
	Cu−Cu	2.6 ± 1.1	2.49 ± 0.02	104 ± 39		
	Cu−Au	2.2 ± 1.1	2.59 ± 0.03	73 ± 38		

Analysis of the EXAFS region provides information regarding the adsorption site of the Cu atoms on the Au surface from the Cu−Au coordination number and information regarding the packing of the Cu atoms in the upd layer from Cu−Cu coordination number.

The XANES region of the Cu K edge XAS spectrum (Figure 8) shows a clear change in features near the edge as the potential is decreased, especially the appearance of a pre-edge peak at 8980 eV, which is present in the XANES of the Cu foil. At −0.21 V, there is a slight increase in the amplitude of the XANES below the main peak of the edge, indicating some reduction of the Cu^{2+}, but little shift in the position of the edge or the main peak in the XANES at 8996 eV. As the potential is made more negative, to −0.42 V (orange line) and then −0.51 V (red line), this shift continues, but the XANES spectrum never fully reproduces all of the features of that obtained for the metallic Cu foil. It has previously been reported[28,29] that, following deposition, the Cu^{2+} does not fully discharge to Cu^0, which is consistent with the findings reported here. However, this also means that the XANES analysis alone is unable to provide quantification of the fraction of the copper in the beam path deposited as the upd layer at each potential, where the total amount consists of the sum of the ions in solution and the (partially) discharged (ions) on the surface.

The k^2 weighted in situ EXAFS data and corresponding Fourier transforms acquired at 300 K are shown in Figure 9, and the corresponding fit parameters are presented in Table 4. The fits to the data at +0.20 and −0.21 V show Cu−O first shell neighbors consistent with octahedrally coordinated Cu^{2+} ions. In contrast to previously reported studies of Cu upd on bulk Au,[22] no Cu−Cu or Cu−Au contributions could be fit to the EXAFS at −0.21 V (resulting in negative coordination numbers and/or disorder terms). This suggests that, although some reduction of the Cu was detected in the XANES at −0.21 V, either the proportion of Cu deposited onto the Au nanoparticles was insufficient to be detected in the presence of the Cu^{2+} in the solution or the initial Cu upd layer is not metallic in its coordination.

Fitting the Cu K edge EXAFS data at −0.42 V required both Cu−O and Cu−Au neighbors. A gradual decrease in the coordination number and distance for the first Cu−O neighbor is observed as the potential is made more negative from +0.20 to −0.42 V. The ordered structures proposed for Cu deposition on Au single-crystal surfaces[22,29] were used as the initial fitting models; however, these did not give realistic EXAFS fit results. At −0.42 V, a complete Cu monolayer was reported on the single-crystal surface (see Figure 1b for the structure on Au(111)), with sulfate atop the Cu.[20,22,23,32,33] If this structure was present for the nanoparticle catalyst, there should now be Cu−O, Cu−Cu, and Cu−Au contributions to the first coordination shell; however, no Cu−Cu contribution was found.

In the experiment reported here at −0.42 V, both Cu^{2+} in solution and the expected Cu and SO_4^- adlayer forming on the surface will be present. Therefore, two different Cu−O environments are expected. This multiplicity of Cu−O environments at similar distances is likely to account for the large increase in the Debye−Waller (disorder) term for the Cu−O shell at −0.42 V as

dx.doi.org/10.1021/ja206763e |J. Am. Chem. Soc. 2011, 133, 19448–19458

compared to the values obtained at the more positive potentials. The quantity and quality of available data prohibit fitting multiple Cu−O neighbors at similar distances to enable a more precise determination of the Cu−O environments (limited by the Nyquist criterion).

The large Cu−Au first shell coordination number and lack of Cu−Cu first shell coordination numbers obtained from fitting the data at −0.42 V are also inconsistent with the structures reported on the different Au crystal surfaces,[20,22,23,32,33] with the lack of Cu−Cu indicating that the formation of the Cu upd shell is far from complete. As mentioned earlier, no Au−Cu neighbors were found in the corresponding fit to the data obtained at the Au L_3 edge at −0.42 V. The Au EXAFS data are expected to be far less sensitive to the presence of a monolayer of Cu on the surface, with a complete additional shell on the 3.8 nm diameter particles yielding an expected Au−Cu coordination number of 1.9. Combining the complete absence of any Au−Cu neighbors at this potential and the large Cu−Au coordination number confirms that the Cu that has been deposited is retained on the surface of the Au nanoparticles. The number of Cu−Au neighbors, 6.44 ± 2.41, suggests that the Cu is preferentially depositing in defects in the outer shell of the surface of the Au nanoparticles, as shown in Figure 10.

The Cu coverage was measured using the stripping voltammograms (Figure 11) by comparison with the surface area of the Au nanoparticles determined from the charge, 61.32 mC, associated with Au−O stripping peak at +0.45 V (Figure 5), and assuming that both Au−O formation/stripping and Cu adsorption/desorption are 2 electron processes. After holding the potential for 30 min at −0.42 V, a charge of 27.15 mC was obtained, corresponding to a coverage of θ_{Cu} = 0.44. The Cu^{2+} ion concentration was greatly in excess of that required to form the complete monolayer, and, therefore, the lack of available Cu^{2+} is not the source of the incomplete coverage at this potential. After holding at −0.51 V, a charge of 62.77 mC was obtained, corresponding to slightly more than that required for a full monolayer, θ_{Cu} = 1.02.

At −0.51 V, the fit to the Cu K edge EXAFS data required both Cu−Cu and Cu−Au first shell neighbors, but no longer required Cu−O neighbors, indicating a transition to a much more metallic coordination environment. The total first shell coordination number (sum of Cu−Cu and Cu−Au coordination numbers) remained low, much less than the 12 first shell neighbors that would be present for bulk Cu in the fcc structure, and the Au L_3 EXAFS continued to be possible to fit without Au−Cu neighbors. Taken together, these results verify that the Cu was still confined to the surface of the Au nanoparticles. The lack of Au−Cu neighbors also indicates that the Cu may be clustering together in areas on the Au nanoparticle surface, rather than forming a more evenly distributed/complete shell around the Au, as is commonly assumed when the Cu upd layer sacrificial layer is prepared for use in the subsequent galvanic replacement approach to the preparation of core−shell electrocatalyst nanoparticles. A similar effect has been predicted for Ag upd on Au(100) surfaces, with small islands tending to form on the Au surface rather than a uniform monolayer.[69]

In contrast to previously reported studies of Cu upd on massive single-crystal Au surfaces,[22,23,29] the analysis of the EXAFS data presented above is inconsistent with the formation of an ordered overlayer structure at all of the potentials considered. At −0.21 V, where on the single-crystal surface a mixed layer of adsorbed Cu and SO_4^{2-} ions was found, we found no direct evidence of Cu deposition onto the surface of the Au nanoparticles, although the XANES did show a minority presence of reduced Cu species. At −0.42 V, where the single-crystal studies found the complete Cu upd layer topped by a layer of adsorbed SO_4^{2-}, the Cu K edge EXAFS data for deposition on Au/C catalyst were consistent with Cu deposition at defect sites on the surface of the Au nanoparticles, representing a coverage of θ_{Cu} = 0.44. This was further supported by the Au L_3 edge EXAFS data, where the fits did not require the addition of Au−Cu neighbors, indicating that the Cu was deposited on the surface of the Au. Finally, at −0.51 V, where bulk Cu deposition would be found at the single-crystal Au surface, the data reported here for deposition on the nanoparticles indicate that the Cu shell remained incomplete, with the Cu forming clusters on the Au surface.

The findings reported here have profound implications for the use of sacrificial Cu upd layers in the preparation of core (often Au)−shell electrocatalysts by galvanic replacement of the Cu, if the formation of a complete shell is required to obtain the optimal activity or stability of the resulting core−shell material. As mentioned earlier, such difficulties appear to have been acknowledged by Wang et al.[5] in their preparation of a Pd core−Pt shell catalyst where they describe a modification of the Cu upd method,

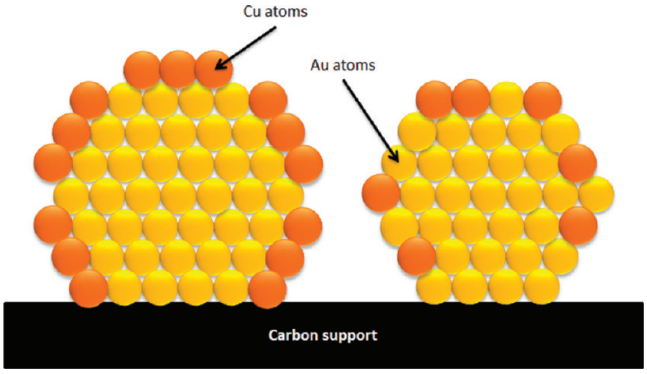

Figure 10. Schematic of Cu deposition on Au nanoparticle based on an idealized complete outer shell (left) and an incomplete outer shell (right).

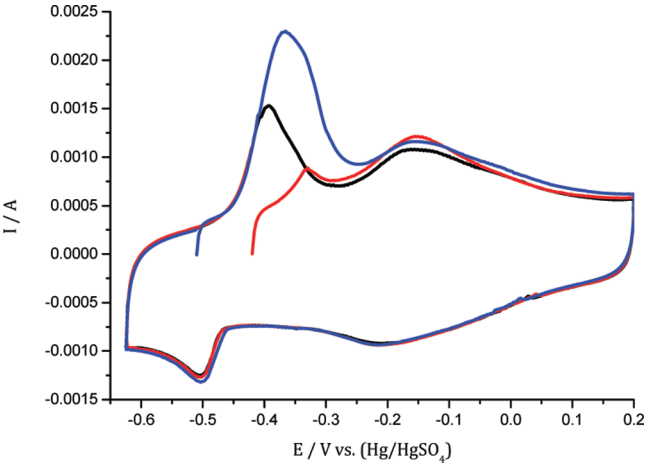

Figure 11. Stripping voltammograms for the 4 wt % Au/C electrode in 0.5 M H_2SO_4 and 2 mM $CuSO_4$ at a sweep rate of 5 mV s^{-1}. Standard voltammogram (black), stripping after −0.42 V hold for 30 min (red), and stripping after −0.51 V hold for 30 min (blue).

using Cu deposition and stripping in the presence of Pt^{2+} to obtain a more uniform Pt coverage of the core. However, many of the reports of core−shell catalyst preparation using the galvanic replacement technique do not appear to take such difficulties into account, and, therefore, their assumptions regarding the true structure of the resulting catalyst materials must be treated with caution.

CONCLUSIONS

We have presented the first in situ EXAFS study of Cu upd on a supported Au nanoparticle catalyst. Investigation of the potential dependence of the structure of the Au/C substrate catalyst using EXAFS data collected at the Au L_3 edge showed that the shape of the catalyst particles is potential dependent, best represented as a flattened spherical structure at positive potentials and being approximately spherical at the negative potentials where Cu upd occurs. By obtaining and analyzing EXAFS data at both the Au L_3 and the Cu K edges, a comprehensive view of the structure of the Cu upd layer at each potential was obtained. In contrast to the single-crystal studies reported previously, no evidence for a mixed sulfate/Cu upd layer at −0.21 V (no Cu−Cu or Cu−Au neighbors in the Cu K EXAFS or Au−Cu neighbors in the Au L_3 EXAFS) was found, although the Cu K edge XANES data did indicate some reduction of the copper species. At −0.42 V, where a complete Cu monolayer is predicted from the single-crystal studies, only a partial monolayer was found with the Cu atoms that were deposited being preferentially located in defect sites on the surface of the Au particles (large Cu−Au and no Cu−Cu coordination numbers in the Cu K edge EXAFS, with no Au−Cu neighbors found in the Au L_3 EXAFS). Finally, at −0.51 V, where bulk Cu deposition was anticipated, the structure was found to be more accurately represented as Cu clusters on the surface of the Au nanoparticles than as a complete/uniform shell (increased Cu−Cu and decreased Cu−Au coordination numbers in the Cu K EXAFS, with no Au−Cu neighbors in the Au L_3 EXAFS). These findings indicate that Cu upd deposition on Au nanoparticle surfaces may not yield the uniform shell structure required to achieve good core−shell structures following a single galvanic replacement step and that further structural characterization of the final product catalyst is required to verify that the core−shell structure was achieved.

AUTHOR INFORMATION

Corresponding Author
a.e.russell@soton.ac.uk

ACKNOWLEDGMENT

We would like to thank Dr. Bruce Ravel of the NSLS for the excellent beamline support, and Dr. Tim Hyde and Dr. Don Ozkaya of Johnson Matthey Technology Centre, Sonning Common, for the XRD and TEM measurements. This work has been made possible by the financial support of the EPSRC and Johnson Matthey. Use of the National Synchrotron Light Source, Brookhaven National Laboratory, was supported by the U.S. Department of Energy, Office of Science, Office of Basic Energy Sciences, under Contract No. DE-AC02-98CH10886.

REFERENCES

(1) Vielstich, W.; Lamm, A.; Gasteiger, H. A. *Handbook of Fuel Cells: Fundamentals, Technology, Applications*; Wiley: New York, 2003; Vol. 3.
(2) Gasteiger, H. A.; Marković, N. M. *Science* **2009**, *324*, 48.
(3) Gasteiger, H. A.; Kocha, S. S.; Sompalli, B.; Wagner, F. T. *Appl. Catal., B* **2005**, *56*, 9.
(4) Oviedo, O. A.; Leiva, E. P. M.; Mariscal, M. M. *Phys. Chem. Chem. Phys.* **2008**, *10*, 3561.
(5) Wang, J. X.; Inada, H.; Wu, L.; Zhu, Y.; Choi, Y.; Liu, P.; Zhou, W.-P.; Adzic, R. R. *J. Am. Chem. Soc.* **2009**, *131*, 17298.
(6) Zhang, J.; Lima, F. H. B.; Shao, M. H.; Sasaki, K.; Wang, J. X.; Hanson, J.; Adzic, R. R. *J. Phys. Chem. B* **2005**, *109*, 22701.
(7) Shao, M.; Sasaki, K.; Marinkovic, N. S.; Zhang, L.; Adzic, R. R. *Electrochem. Commun.* **2007**, *9*, 2848.
(8) Oviedo, O. A.; Mariscal, M. M.; Leiva, E. P. M. *Electrochim. Acta* **2010**, *55*, 8244.
(9) Zhang, G.; Kuang, Y.; Liu, J.; Cui, Y.; Chen, J.; Zhou, H. *Electrochem. Commun.* **2010**, *12*, 1233.
(10) Knupp, S.; Vukmirovic, M.; Haldar, P.; Herron, J.; Mavrikakis, M.; Adzic, R. *Electrocatalysis* **2010**, *1*, 213.
(11) Zhang, J.; Mo, Y.; Vukmirovic, M. B.; Klie, R.; Sasaki, K.; Adzic, R. R. *J. Phys. Chem. B* **2004**, *108*, 10955.
(12) Zhang, J.; Vukmirovic, M. B.; Xu, Y.; Mavrikakis, M.; Adzic, R. R. *Angew. Chem., Int. Ed.* **2005**, *44*, 2132.
(13) Brankovic, S. R.; Wang, J. X.; Adzic, R. R. *Surf. Sci.* **2001**, *474*, L173.
(14) Markovic, N. M.; Ross, P. N. *Surf. Sci. Rep.* **2002**, *45*, 121.
(15) Solla-Gullon, J.; Rodriguez, P.; Herrero, E.; Aldaz, A.; Feliu, J. M. *Phys. Chem. Chem. Phys.* **2008**, *10*, 1359.
(16) Kibler, L. A.; Kolb, D. M. *Z. Phys. Chem.* **2003**, *217*, 1265.
(17) Feliu, J. M.; Orts, J. M.; Llorca, M. J.; Gomez, R.; Clavilier, J. *An. Quim.* **1993**, *89*, 407.
(18) Aldaz, A.; Clavilier, J.; Feliu, J. M. *J. Phys. IV* **1994**, *4*, 75.
(19) Francke, R.; Climent, V.; Baltruschat, H.; Feliu, J. M. *J. Electroanal. Chem.* **2008**, *624*, 228.
(20) Kuzume, A.; Herrero, E.; Feliu, J. M.; Nichols, R. J.; Schiffrin, D. J. *J. Electroanal. Chem.* **2004**, *570*, 157.
(21) Tamura, K.; Oyanagi, H.; Kondo, T.; Koinuma, M.; Uosaki, K. *J. Phys. Chem. B* **2000**, *104*, 9017.
(22) Lee, J. R. I.; O'Malley, R. L.; O'Connell, T. J.; Vollmer, A.; Rayment, T. *J. Phys. Chem. C* **2009**, *113*, 12260.
(23) Blum, L.; Abruna, H. D.; White, J.; Gordon, J. G.; Borges, G. L.; Samant, M. G.; Melroy, O. R. *J. Chem. Phys.* **1986**, *85*, 6732.
(24) Magnussen, O. M.; Hotlos, J.; Nichols, R. J.; Kolb, D. M.; Behm, R. J. *Phys. Rev. Lett.* **1990**, *64*, 2929.
(25) Shi, Z.; Lipkowski, J. *J. Electroanal. Chem.* **1994**, *365*, 303.
(26) Nakamura, M.; Endo, O.; Ohta, T.; Ito, M.; Yoda, Y. *Surf. Sci.* **2002**, *514*, 227.
(27) Kim, Y.-G.; Kim, J. Y.; Vairavapandian, D.; Stickney, J. L. *J. Phys. Chem. B* **2006**, *110*, 17998.
(28) Omar, I. H.; Pauling, H. J.; Juttner, K. *J. Electrochem. Soc.* **1993**, *140*, 2187.
(29) Toney, M. F.; Howard, J. N.; Richer, J.; Borges, G. L.; Gordon, J. G.; Melroy, O. R.; Yee, D.; Sorensen, L. B. *Phys. Rev. Lett.* **1995**, *75*, 4472.
(30) Cuesta, A.; Kleinert, M.; Kolb, D. M. *Phys. Chem. Chem. Phys.* **2000**, *2*, 5684.
(31) Cappadonia, M.; Robinson, K. M.; Schmidberger, J.; Stimming, U. *J. Electroanal. Chem.* **1997**, *436*, 73.
(32) Möller, F.; Magnussen, O. M.; Behm, R. J. *Electrochim. Acta* **1995**, *40*, 1259.
(33) Möller, F.; Magnussen, O. M.; Behm, R. J. *Phys. Rev. B* **1995**, *51*, 2484.
(34) Ikemiya, N.; Miyaoka, S.; Hara, S. *Surf. Sci.* **1995**, *327*, 261.
(35) Brankovic, S. R.; Wang, J. X.; Adzic, R. R. *J. Serb. Chem. Soc.* **2001**, *66*, 887.
(36) Sasaki, K.; Mo, Y.; Wang, J. X.; Balasubramanian, M.; Uribe, F.; McBreen, J.; Adzic, R. R. *Electrochim. Acta* **2003**, *48*, 3841.
(37) Vukmirovic, M. B.; Zhang, J.; Sasaki, K.; Nilekar, A. U.; Uribe, F.; Mavrikakis, M.; Adzic, R. R. *Electrochim. Acta* **2007**, *52*, 2257.
(38) Sasaki, K.; Naohara, H.; Cai, Y.; Choi, Y. M.; Liu, P.; Vukmirovic, M. B.; Wang, J. X.; Adzic, R. R. *Angew. Chem., Int. Ed.* **2010**, *49*, 8602.

(39) Tessier, B. C.; Russell, A. E.; Theobald, B. R.; Thompsett, D. *ECS Trans.* **2009**, *16*, 1.
(40) Kinoshita, K. *J. Electrochem. Soc.* **1990**, *137*, 845.
(41) Jin, Y.; Shen, Y.; Dong, S. *J. Phys. Chem. B* **2004**, *108*, 8142.
(42) Seo, D.; Park, J. H.; Jung, J.; Park, S. M.; Ryu, S.; Kwak, J.; Song, H. *J. Phys. Chem. C* **2009**, *113*, 3449.
(43) Hernández, J.; Solla-Gullón, J.; Herrero, E.; Aldaz, A.; Feliu, J. M. *J. Phys. Chem. B* **2005**, *109*, 12651.
(44) Sánchez-Sánchez, C. M.; Vidal-Iglesias, F. J.; Solla-Gullón, J.; Montiel, V.; Aldaz, A.; Feliu, J. M.; Herrero, E. *Electrochim. Acta* **2010**, *55*, 8252.
(45) Personick, M. L.; Langille, M. R.; Zhang, J.; Mirkin, C. A. *Nano Lett.* **2011**, *11*, 3394.
(46) Tran, T. T.; Lu, X. *J. Phys. Chem. C* **2011**, *115*, 3638.
(47) Hernández, J.; Solla-Gullón, J.; Herrero, E.; Aldaz, A.; Feliu, J. M. *J. Phys. Chem. C* **2007**, *111*, 14078.
(48) Xiang, Y.; Wu, X.; Liu, D.; Feng, L.; Zhang, K.; Chu, W.; Zhou, W.; Xie, S. *J. Phys. Chem. C* **2008**, *112*, 3203.
(49) Calvin, S.; Miller, M. M.; Goswami, R.; Cheng, S. F.; Mulvaney, S. P.; Whitman, L. J.; Harris, V. G. *J. Appl. Phys.* **2003**, *94*, 778.
(50) Frenkel, A. I. *J. Synchrotron Radiat.* **1999**, *6*, 293.
(51) Russell, A. E.; Rose, A. *Chem. Rev.* **2004**, *104*, 4613.
(52) Rose, A.; Bilsborrow, R.; King, C. R.; Ravikumar, M. K.; Qian, Y.; Wiltshire, R. J. K.; Crabb, E. M.; Russell, A. E. *Electrochim. Acta* **2009**, *54*, 5262.
(53) Rose, A.; Crabb, E. M.; Qian, Y.; Ravikumar, M. K.; Wells, P. P.; Wiltshire, R. J. K.; Yao, J.; Bilsborrow, R.; Mosselmans, F.; Russell, A. E. *Electrochim. Acta* **2007**, *52*, 5556.
(54) Crabb, E. M.; Ravikumar, M. K.; Thompsett, D.; Hurford, M.; Rose, A.; Russell, A. E. *Phys. Chem. Chem. Phys.* **2004**, *6*, 1792.
(55) Brust, M.; Walker, M.; Bethell, D.; Schriffin, D. J.; Whyman, R. *J. Chem. Soc., Chem. Commun.* **1994**, 801.
(56) Ravel, B.; Newville, M. *J. Synchrotron Radiat.* **2005**, *12*, 537.
(57) Rehr, J. J.; Albers, R. C.; Zabinsky, S. I. *Phys. Rev. Lett.* **1992**, *69*, 3397.
(58) Newville, M. *J. Synchrotron Radiat.* **2001**, *8*, 96.
(59) Newville, M.; Limacrvincedilscaron, P.; Yacoby, Y.; Rehr, J. J.; Stern, E. A. *Phys. Rev. B* **1993**, *47*, 14126.
(60) Frenkel, A. *J. Synchrotron Radiat.* **1999**, *6*, 293.
(61) Roldan Cuenya, B.; Croy, J. R.; Mostafa, S.; Behafarid, F.; Li, L.; Zhang, Z.; Yang, J. C.; Wang, Q.; Frenkel, A. I. *J. Am. Chem. Soc.* **2010**, *132*, 8747.
(62) Benfatto, M.; D'Angelo, P.; Della Longa, S.; Pavel, N. V. *Phys. Rev. B* **2002**, *65*, 174205.
(63) Inada, Y.; Ozutsumi, K.; Funahashi, S.; Soyama, S.; Kawashima, T.; Tanaka, M. *Inorg. Chem.* **1993**, *32*, 3010.
(64) Korshin, G. V.; Frenkel, A. I.; Stern, E. A. *Environ. Sci. Technol.* **1998**, *32*, 2699.
(65) Kelly, S. D.; Hesterberg, D.; Ravel, B. *Methods of Soil Analysis Part 5. Mineralogical Methods*; Soil Science Society of America: Madison, WI, 2008; p 444.
(66) Jentys, A. *Phys. Chem. Chem. Phys.* **1999**, *1*, 4059.
(67) Solliard, C.; Flueli, M. *Surf. Sci.* **1985**, *156*, 487.
(68) Marsh, J. H.; Orchard, S. W. *Carbon* **1992**, *30*, 895.
(69) Gimenez, M. C.; Del Popolo, M. G.; Leiva, E. P. M.; Garcia, S. G.; Salinas, D. R.; Mayer, C. E.; Lorenz, W. J. *J. Electrochem. Soc.* **2002**, *149*, E109.